Photoacoustics 36 (2024) 100592

Contents lists available at ScienceDirect

Photoacoustics

journal homepage: www.elsevier.com/locate/pacs

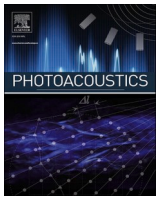

High-sensitivity methane detection based on QEPAS and H-QEPAS technologies combined with a self-designed 8.7 kHz quartz tuning fork

Tiantian Liang [a,b], Shunda Qiao [a,b], Yanjun Chen [a,b], Ying He [a,b], Yufei Ma [a,b,*]

[a] National Key Laboratory of Science and Technology on Tunable Laser, Harbin Institute of Technology, Harbin 150001, China
[b] Zhengzhou Research Institute, Harbin Institute of Technology, Zhengzhou 450000, China

ARTICLE INFO

Keywords:
CH_4 detection
Self-designed quartz tuning fork
Quartz-enhanced photoacoustic spectroscopy
Heterodyne quartz-enhanced photoacoustic spectroscopy

ABSTRACT

Methane (CH_4) is a greenhouse gas as well as being flammable and explosive. In this manuscript, quartz-enhanced photoacoustic spectroscopy (QEPAS) and heterodyne QEPAS (H-QEPAS) exploring a self-designed quartz tuning fork (QTF) with resonance frequency (f_0) of ~8.7 kHz was utilized to achieve sensitive CH_4 detection. Compared with the standard commercial 32.768 kHz QTF, this self-designed QTF with a low f_0 and large prong gap has the merits of long energy accumulation time and low optical noise. The strongest line located at 6057.08 cm^{-1} in the $2\nu_3$ overtone band of CH_4 was chosen as the target absorption line. A diode laser with a high output power of > 30 mW was utilized as the excitation source. Acoustic micro-resonators (AmRs) were added to the sensor architecture to amplify the intensity of acoustic waves. Compared to the bare QTF, after the addition of AmRs, a signal enhancement of 149-fold and 165-fold were obtained for QEPAS and H-QEPAS systems, respectively. The corresponding minimum detection limits (MDLs) were 711 ppb and 1.06 ppm for QEPAS and H-QEPAS sensors. Furthermore, based on Allan variance analysis the MDLs can be improved to 19 ppb and 27 ppb correspondingly. Compared to the QEPAS sensor, the H-QEPAS sensor shows significantly shorter measurement timeframes, allowing for measuring the gas concentration quickly while simultaneously obtaining f_0 of QTF.

1. Introduction

Methane (CH_4), as an important carbon-based resource, is closely related to human life and widely utilized in various fields, such as energy [1,2], medical diagnosis [3,4], chemical industry [5,6], and so on. However, CH_4 deserves special attention during extraction, transportation and use. On the one hand, CH_4 is not only the second most significant greenhouse gas in the world next to carbon dioxide (CO_2) [7], but its Global Warming Potential (GWP) is 34 times greater than CO_2 on a century timescale [8]. According to statistics, CH_4 concentration in the atmosphere reached 1922.26 ppb by May 2023, which is more than 260% of pre-industrial levels [9]. Unnoticed methane leaks from both biosphere and anthropogenic activity further contribute to the global greenhouse effect [10]. Additionally, CH_4 is a colorless, odorless, non-toxic, but flammable gas, with lower and upper explosive limit concentrations of 4.95% and 14.95% respectively [11]. When the concentration of CH_4 falls within this range and encounters an open flame, it can cause an explosion. Therefore, real-time detection of CH_4 content is crucial.

Various technologies for gas detection such as the thermal, mechanical, electrochemical, and optical have been developed in recent years [12–23]. Among these, laser absorption spectroscopy (LAS) stands out as an optical technology that offers numerous benefits compared to others, such as fast responses, long-term stability, low baseline drift, and high sensitivity and selectivity [24–32]. Quartz-enhanced photoacoustic spectroscopy (QEPAS) is a commonly utilized LAS based gas sensing technology, which was first proposed in 2002 [33]. In QEPAS method, after absorbing the specific wavelength of the laser, the target gas molecules will release heat to the surrounding environment through the non-radiative transition. Based on the photoacoustic effect [34], the continuous emission of acoustic waves will occur at the position of contact between the laser and the gas molecules due to the periodic modulated light beam [35–39]. These acoustic waves will induce vibrations in the detector of quartz tuning fork (QTF) within QEPAS sensing system, thereby exploiting its piezoelectric effect to generate the piezoelectric signal on its surface that can be utilized for gas concentration inversion. Compared to traditional acoustic detection devices, such as microphone [40–43], QTF possesses the advantages of high

* Corresponding author at: National Key Laboratory of Science and Technology on Tunable Laser, Harbin Institute of Technology, Harbin 150001, China.
E-mail address: mayufei@hit.edu.cn (Y. Ma).

https://doi.org/10.1016/j.pacs.2024.100592
Received 12 November 2023; Received in revised form 23 January 2024; Accepted 23 January 2024
Available online 26 January 2024

Q-factor, narrow bandwidth, strong anti-noise capability, affordability, and compact size [44–48]. Consequently, QEPAS technology gained significant attention in the field of gas sensing [49–51].

The resonance frequency (f_0) of QTF is a very important parameter for QEPAS based gas sensing. It determines the frequency for laser modulation and signal demodulation, and therefore it should be calibrated frequently, especially when the environment such as pressure and temperature changes. However, the frequency calibration in traditional QEPAS not only interrupts the monitoring process but also consumes a significant amount of time. The heterodyne quartz-enhanced photoacoustic spectroscopy (H-QEPAS), also known as beat frequency quartz-enhanced photoacoustic spectroscopy (BF-QEPAS), was initially put forward in 2017 by Dong et al. [49], offering the capability to simultaneously measure both gas concentration and f_0 of QTF in just a few seconds [52,53]. By using H-QEPAS technology to measure QTF frequency, the monitoring process remains uninterrupted and the time needed for frequency calibration is greatly reduced.

In this manuscript, a highly sensitive CH_4 sensor based on QEPAS and H-QEPAS technologies was demonstrated respectively. A self-designed QTF with a low resonance frequency of ~8.7 kHz and a large prong gap possessing the merits of long energy accumulation time and low optical noise was employed as the acoustic wave detector. A continuous wave, distributed feedback (CW-DFB) diode laser operating at a center emission wavelength of 1650.96 nm with a high output power of > 30 mW was utilized as the excitation source. A set of acoustic micro-resonators (AmRs) were incorporated on both sides of the QTF to amplify the intensity of acoustic waves. The enhancement effect of different sizes of AmRs was measured separately in the two sensors. Detailed research for CH_4 sensing was performed.

2. Experimental setup

It is crucial for QEPAS system to carefully choose the gas absorption line taking into consideration compatibility with the existing laser source, minimal overlap with other gas absorption lines, and maximizing line strength. Given the well-developed manufacturing technology for DFB laser diodes in the near-infrared band [54,55], the $2\nu_3$ overtone band of CH_4 around 1660 nm is noticed [56]. According to the HITRAN 2020 database [57], simulations were conducted for CH_4's absorption coefficient in this band at 296 K temperature, 1 atm pressure, and a 1 cm optical path length. As shown in Fig. 1(a), the absorption line located at 6057.08 cm^{-1} (1650.96 nm) with the strongest line strength within this band was selected as the target absorption line. To avoid

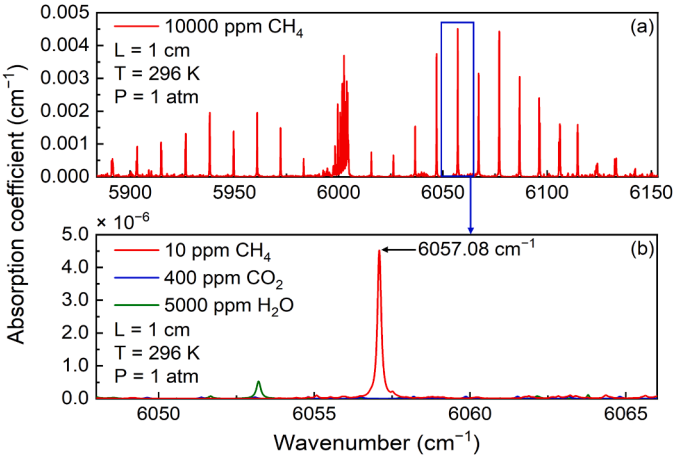

Fig. 1. Simulation for absorption coefficient based on the HITRAN 2020 database at 296 K temperature, 1 atm pressure, and 1 cm optical path length. (a) The $2\nu_3$ overtone band of CH_4 around 6024 cm^{-1}. (b) The comparison of absorption coefficient of CH_4, CO_2 and H_2O in the range from 6048 to 6066 cm^{-1}.

interference from common atmospheric gases, simulations for absorption coefficien were performed for CO_2 and H_2O. As depicted in Fig. 1 (b), there is negligible overlap among CH_4, CO_2 and H_2O.

A CW-DFB diode laser with a center emission wavenumber of 6057.08 cm^{-1} was employed as an excitation source to excite the target line. The output characteristic curve of the used laser is presented in Fig. 2. As the injection current increases, the output power exhibits an upward trend whereas the emission wavenumber of the laser shows a downward trend. When it is operated at a temperature of 31 ℃ and an injection current of 162.9 mA, the laser's emission wavenumber coincides with the target CH_4 absorption line.

The schematic diagram of both QEPAS and H-QEPAS sensing systems is illustrated in Fig. 3. The laser emitted from the pigtail is collimated first by a fiber collimator. The beam enters the gas cell and passes through the two AmRs and QTF. The gap between the two prongs of QTF is 1.73 mm, which is larger than the usually used QTF and is beneficial to reducing optical loss and noise [58,59]. Ultimately the laser beam is detected by a power meter to monitor the optical alignment. The absorption of the modulated laser by the gas molecules in the gas cell generates acoustic waves that induce vibration in the QTF. The presence of AmRs enhances the vibration amplitude on the QTF, resulting in a larger piezoelectric signal and better detection performance [60–62]. This signal is subsequently demodulated with a lock-in amplifier. In the QEPAS system, wavelength modulation and second harmonic ($2f$) demodulation technology were employed to suppress effectively background noise. A high-frequency sine wave and a low-frequency ramp wave were combined and then sent into the laser controller for wavelength modulation of the diode laser. To obtain the steady-state response of QTF, a long period (~ 1 min) ramp wave is often used to sweep the entire gas absorption line. The frequency of the sine wave is set to half of the resonance frequency ($f_0/2$) of the used QTF. By employing lock-in amplifier demodulation, the peak value of the $2f$ signal can be utilized for gas concentration retrieval. In the H-QEPAS system, wavelength modulation and first harmonic ($1f$) demodulation technology were adopted. The laser wavelength is concurrently modulated by a high-frequency sine wave and a low-frequency ramp wave, with the latter being divided into fast-scanning stage and stable stage as depicted in Fig. 3. The frequency of the sine wave is denoted as $f_m = f_0 \pm \Delta f$ [49]. When the ramp wave, adding a sine wave with frequency of f_m, rapidly scans across the gas absorption line, it allows for the acquisition of transient response from the QTF itself. The frequency of the transient response signal is equal to the resonance frequency f_0 of the QTF, and its amplitude decays exponentially with time. Subsequently, this signal is demodulated at f_m by a lock-in amplifier, resulting in a heterodyne signal with Δf frequency. Gas concentration inversion can be determined based on the peak value of the heterodyne signal while simultaneously enabling measurement of QTF resonance frequency based on the equation $f_0 = f_m \pm \Delta f$.

3. Results and discussion

The frequency response curve of the self-designed QTF used in this manuscript is illustrated in Fig. 4(a). After square normalization of the measured data, Lorentz fitting was performed. The f_0 was determined to be 8685.44 Hz with a bandwidth $w = 0.85$ Hz for the bare QTF. QTF's quality factor (Q value) could be calculated as $Q = f_0/w \approx 10218$. After adding AmR with length (L) of 18 mm and inner diameter (ID) of 0.9 mm the f_0 and Q of the QTF are remeasured as 8685.22 Hz and 5949, respectively, which is shown in Fig. 4(b). The changes of f_0 and Q resulted from the acoustic coupling between AmR and QTF. In the QEPAS system, the modulation frequency f_m of sine wave was set to $f_0/2$. In the H-QEPAS system, to make sure that the peak value of the heterodyne signal is large enough and the number of positive peaks is sufficient to calculate the QTF frequency, $f_m = f_0 - \Delta f$ was chosen. The ramp wave utilized in the H-QEPAS system had been optimized. The optimized modulation frequency was 0.25 Hz, and the fast-scanning

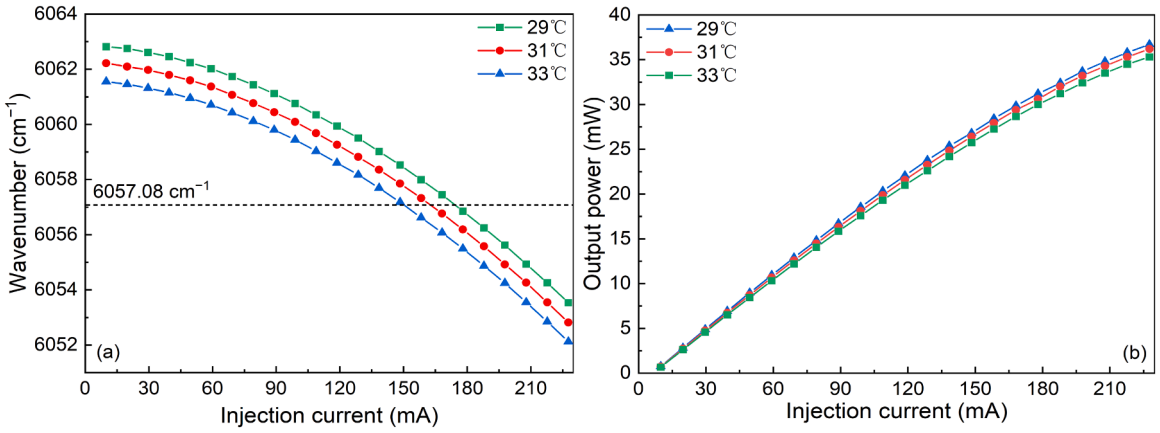

Fig. 2. The output characteristic curve of CW-DFB diode laser for CH_4 sensing. (a) The emission wavenumber varies with the injection current and working temperature. (b) The output power varies with the injection current and working temperature.

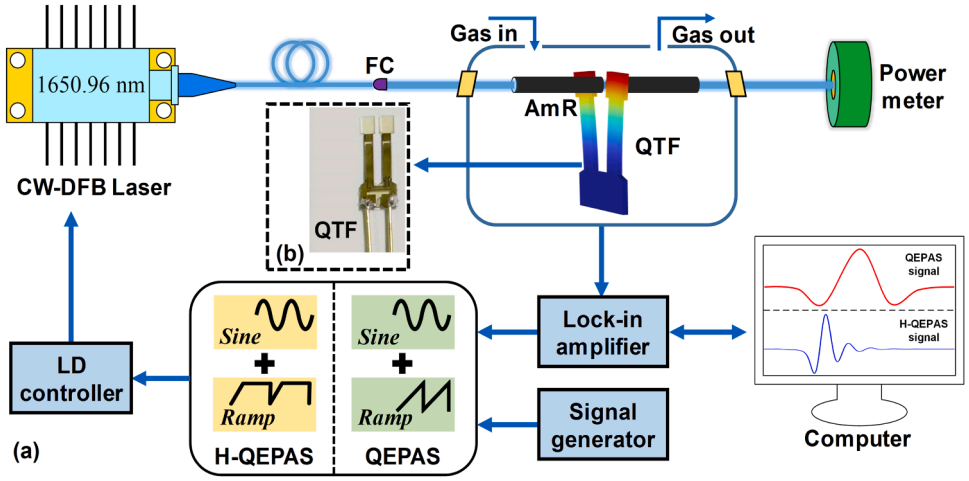

Fig. 3. (a) The schematic diagram of both QEPAS and H-QEPAS systems for CH_4 sensing. (b) The actual image of self-designed QTF.

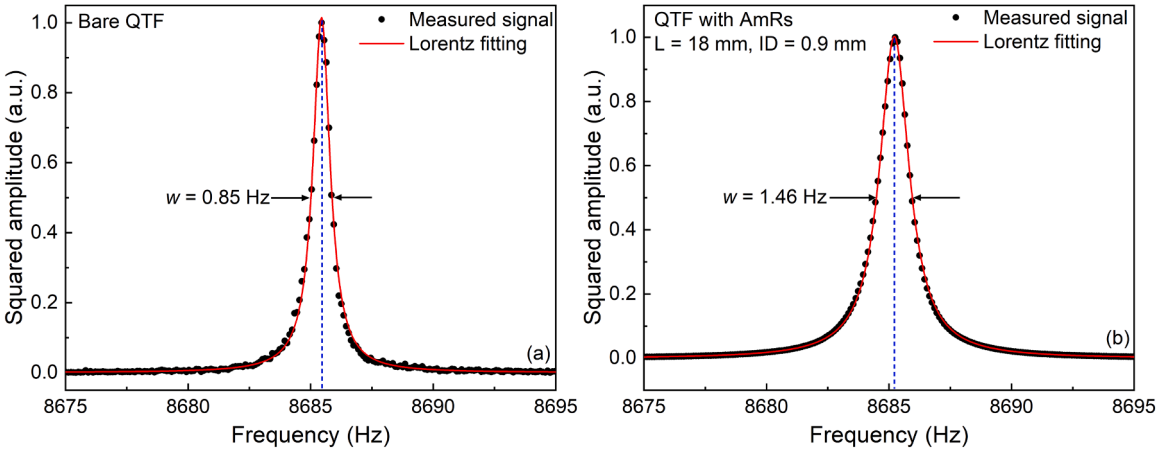

Fig. 4. Frequency response characteristics of the self-designed QTF. (a) Bare QTF. (b) QTF with an *L* of 18 mm and an *ID* of 0.9 mm AmRs.

stage lasted 1.25 s. The filter slope and time constant of the filter in the lock-in amplifier were set to 30 dB/Oct and 20 ms respectively in both systems. The corresponding bandwidth was ~3 Hz which ensures that heterodyne signals with frequency Δf were not filtered out by the filter in lock-in amplifier.

In addition, the modulation depth of sine wave will influence the detection performance [34]. When the operating temperature of the laser is fixed, the laser's emission wavenumber is determined by its injection current. Therefore, the modulation depth of sine wave was replaced by modulation current. The signal amplitudes of both QEPAS and H-QEPAS systems were measured respectively when they changed with the modulation current. As shown in Fig. 5, the signal amplitudes of

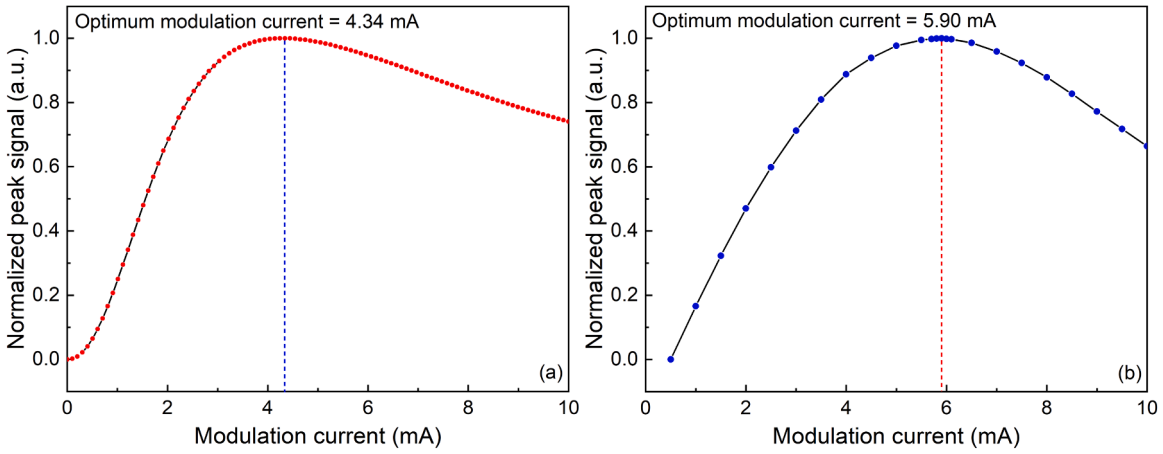

Fig. 5. The curve that depicts the variation of peak signal with the modulation current. (a) QEPAS system. (b) H-QEPAS system.

both systems initially rose and then declined as the modulation current increased. The optimal modulation current of the QEPAS system was determined as 4.34 mA. While for the H-QEPAS system, it was 5.90 mA. The poor high-frequency modulation performance of the CW-DFB laser results in a larger optimal modulation current of the latter [63].

The enhancement effect of QTF vibration is jointly influenced by the size of AmR, including its length (L) and inner diameter (ID). The optimal length (L_{opt}) of AmR depends on f_0 of the used QTF, and it should satisfy $\lambda_s/4 < L < \lambda_s/2$ [60], where λ_s could be calculated as $\lambda_s = c_s/f_0$ and c_s represents the sound velocity in the medium. When assigning a value of 340 m/s to c_s, the range for L_{opt} spans from 9.8 mm to 19.6 mm. To achieve optimal enhancement effect, AmRs with different lengths (L = 17 mm, 18 mm, 19 mm, and 20 mm), different inner diameters (ID = 0.8 mm, 0.9 mm, 1.0 mm, 1.1 mm, 1.3 mm, 1.5 mm, 1.6 mm, and 1.7 mm) and same outer diameters (OD = 2.5 mm) were designed. All kinds of AmRs were made of stainless steel. The coupling degree between QTF and AmRs varies depending on the sizes of the latter. In Fig. 4 (b), taking an example with L = 18 mm and ID = 0.9 mm, the QTF coupled with this set of AmRs exhibited a wider bandwidth of 1.46 Hz, a lower Q value of 5949, and a drift in frequency. Therefore, after each replacement of the set of AmRs, it is necessary to re-calibrate f_0 for the QTF.

To assess the improvement of AmR on the signal level of the QEPAS sensor, measurements were conducted with varying ID and L, as depicted in Fig. 6. When keeping the L constant for AmR, the peak signal value of the QEPAS system initially increased and then decreased as the ID decreased. The optimal ID was determined to be 0.9 mm. Conversely, when maintaining a constant ID for AmR, the signal peak value of the QEPAS system also exhibited an initial increase followed by a decrease with an increase in L. With the exception of the 1.7 mm ID, an optimal L of 19 mm was observed in other IDs of AmRs. However, for an ID of 1.7 mm, an optimal L of 18 mm was found. This is because the L of the optimal AmR gradually increases as the ID decreases [64].

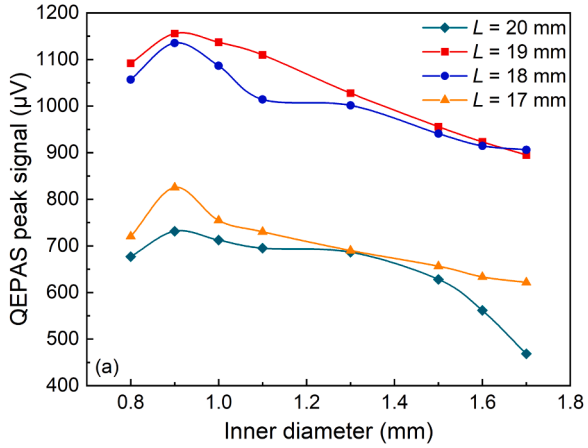

Fig. 6. QEPAS peak signal as a function of L and ID of the AmRs.

With the optimized size configuration for AmR, signals from both QEPAS and H-QEPAS systems were measured at a CH_4 concentration level of 1%. The results are shown in Fig. 7(a) and (b), respectively. The noise levels were separately measured in pure nitrogen (N_2) environments for both QEPAS and H-QEPAS systems, as shown in Fig. 8(a) and (b). The peak value obtained from the bare QTF-based QEPAS signal was recorded as 7.68 μV. However, when utilizing a QTF coupled with optimized AmRs, it increased significantly to 1155.66 μV, resulting in approximately a 149-fold enhancement. The system noise level was calculated to be 82.17 nV while yielding a signal-to-noise ratio (SNR) of 14064 and a minimum detection limit (MDL) of 711 ppb. In the H-QEPAS sensor system, the peak value of the signal obtained using a bare QTF was 4.61 μV. After adding the AmRs with optimum size, the signal peak value increased to 765.20 μV, leading to a 165-fold improvement. The calculated system noise, SNR, and MDL were 81.04 nV, 9442, and 1.06 ppm respectively. The QEPAS system can achieve a lower detection limit, but it requires approximately 1 min to obtain a complete 2f waveform. Whereas the H-QEPAS system can capture the entire heterodyne signal waveform within just 4 s and simultaneously measure f_0 for the QTF. In Fig. 7(b), the heterodyne signal frequency could be calculated as $\Delta f = 1/\Delta t = 1.44$ Hz, and then the f_0 of QTF can be retrieved according to the formula: $f_0 = f_m + \Delta f = 8685.18$ Hz. Compared with the optical excitation method shown in Fig. 4, the measurement error is less than 0.16 Hz.

Finally, the long-term stability for both QEPAS and H-QEPAS sensor systems was evaluated when continuous monitoring of pure N_2 was performed. The Allan deviation plot illustrates the impact of noise on system performance, and it was adopted for both systems. The obtained results are depicted in Fig. 9(a) and (b), respectively. It could be observed that white noise dominates and the Allan deviation decreased with increasing integration time at small integration time. However, as the integration time increased, random-walk drift started to dominate [65]. At this time, the Allan deviation instead increased, indicating an optimal integration time exists. Increasing the integration time of the QEPAS system to 100 s and 4560 s resulted in the MDLs of 103 ppb and 19 ppb, respectively. In contrast, when extending the H-QEPAS system's integration time to 100 s and 3200 s, the corresponding MDLs were 141 ppb and 27 ppb, respectively. In Table 1, we compared the performance obtained through QEPAS and H-QEPAS technologies in other references with the results in this manuscript. The selected CH_4 absorption line reported in this paper is located in the near-infrared band, and the obtained MDL of CH_4-QEPAS sensor is superior to that of the other studies

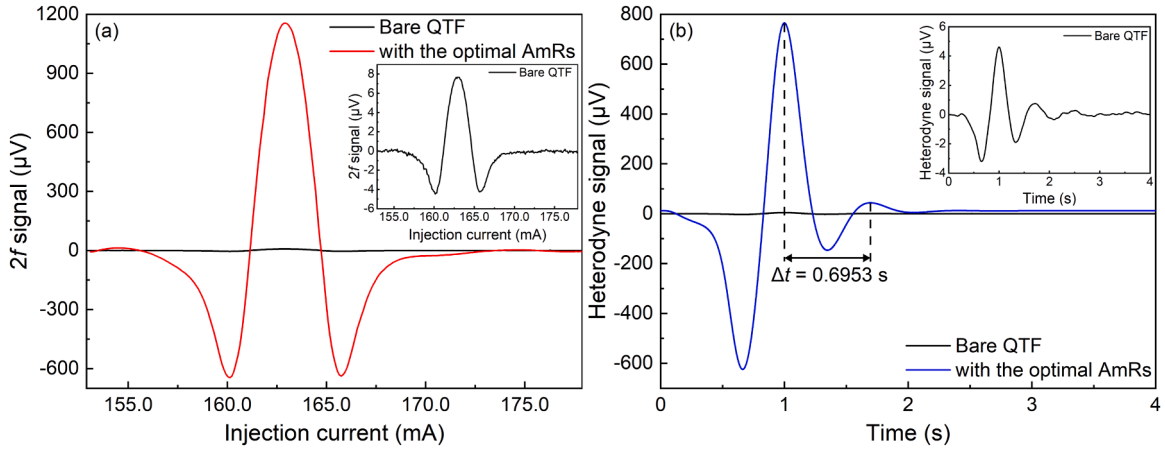

Fig. 7. Comparison between the bare QTF and QTF with AmRs. (a) 2 *f* signal in the QEPAS system. (b) Heterodyne signal in the H-QEPAS system.

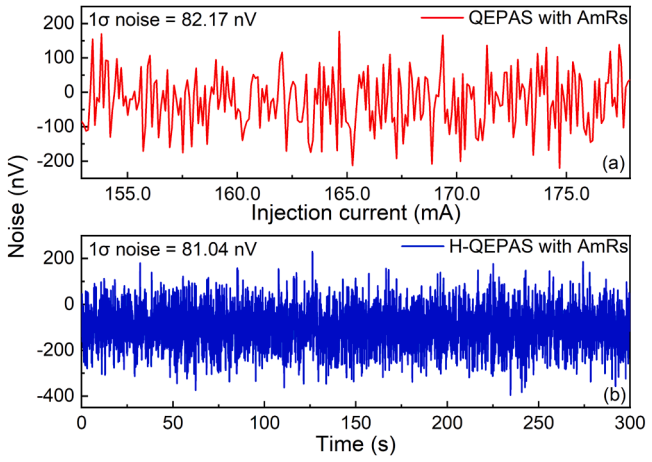

Fig. 8. The measured noise level for the two systems at pure N_2 environments. (a) QEPAS system. (b) H-QEPAS system.

in this band, but not as good as the results in the mid-infrared band because of the stronger absorption of mid-infrared band. The MDL of CH_4 detection using H-QEPAS in this study is better than the literature when H-QEPAS technology is employed.

4. Conclusion

In this paper, highly sensitive detection of CH_4 was achieved based on QEPAS and H-QEPAS technologies, respectively, by utilizing a self-designed QTF with f_0 of ~8.7 kHz. This used QTF has such a low f_0 and big prong gap of 1.73 mm possessing the merits of long energy accumulation time and low optical noise. A CW-DFB diode laser with high output power and a central emission wavelength of 1650.96 nm was selected as the excitation source to match the strongest absorption line of CH_4 in the $2\nu_3$ overtone band. To further enhance the detection performance of CH_4, AmRs were equipped on both sides of the QTF to amplify its vibration amplitude. Through experimental investigation, the optimal size of AmRs was determined, which resulted in an enhancement of signal peak values by a factor of 149-fold and 165-fold compared to the bare QTF for QEPAS and H-QEPAS systems, respectively. The corresponding MDLs for CH_4 detection were 711 ppb and 1.06 ppm for these two sensors. Furthermore, the long-term stability was analyzed using Allan deviation analysis. Increasing the integration time of the QEPAS system to 4560 s led to an MDL improvement down to 19 ppb. In contrast, when the integration time of the H-QEPAS sensor was increased to 3200 s, its MDL improved to 27 ppb. Although slightly inferior in terms of detection performance compared to the QEPAS system, the H-QEPAS system offers advantages such as fast measurement and obtaining f_0 simultaneously along with gas concentration. In future research, we will continue to optimize the shape and size of the tuning fork, while exploring alternative materials with higher piezoelectric coefficients to substitute quartz.

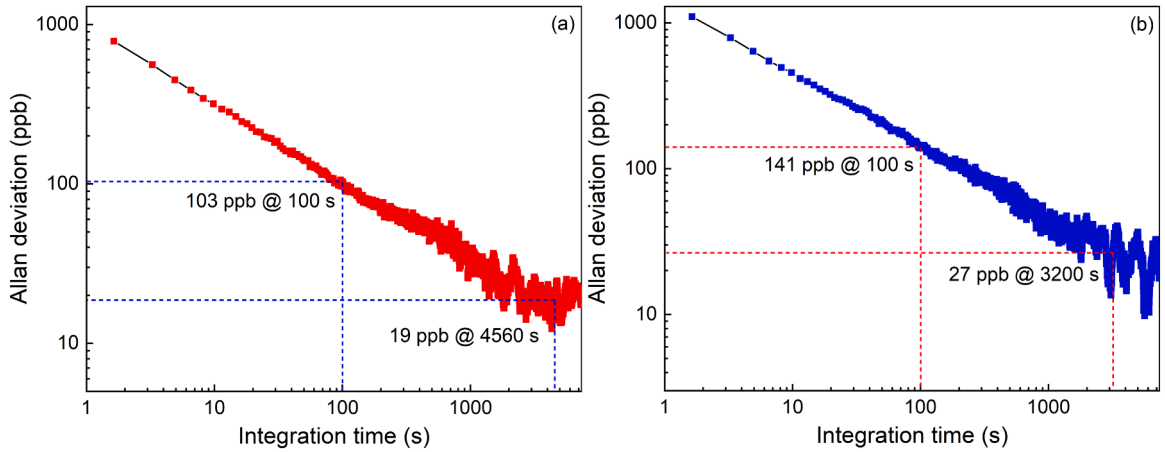

Fig. 9. Allan deviation analysis. (a) QEPAS system. (b) H-QEPAS system.

Table 1
Comparison of CH_4 detection limits in QEPAS and H-QEPAS methods.

Technology	Wave band	Wavenumber (cm^{-1})	MDL (ppm) (@Integration time)	Reference
QEPAS	Near-infrared	6057.08	3.2 (@1 s)	[66]
QEPAS	Near-infrared	4290.22	1.2 (@100 s)	[67]
QEPAS	Near-infrared	6046.95	0.288 (@125 s)	[68]
QEPAS	Mid-infrared	2788.64	55.57 (@1 s)	[49]
QEPAS	Mid-infrared	1275.04	0.028 (@0.1 s)	[69]
QEPAS	Mid-infrared	1295.5	0.048 (@0.1 s)	[70]
QEPAS	Mid-infrared	2989.5	0.09 (@1 s)	[71]
QEPAS	Mid-infrared	3038.5	0.05 (@1 s)	[72]
QEPAS	Mid-infrared	1275.04	0.013 (@1 s)	[73]
QEPAS	Near-infrared	6057.08	0.103 (@100 s)	This study
H-QEPAS	Near-infrared	6046.95	28.35 (@114 s)	[74]
H-QEPAS	Mid-infrared	2788.64	40.75 (@ 1 s)	[49]
H-QEPAS	Near-infrared	6057.08	0.141 (@100 s)	This study

CRediT authorship contribution statement

Ma Yufei: Writing – review & editing, Supervision, Conceptualization. **Chen Yanjun:** Validation. **He Ying:** Resources. **Liang Tiantian:** Writing – original draft, Investigation. **Qiao Shunda:** Formal analysis.

Declaration of Competing Interest

The authors declare that they have no known competing financial interests or personal relationships that could have appeared to influence the work reported in this paper.

Data availability

Data will be made available on request.

Acknowledgments

We are grateful for financial supports from the National Natural Science Foundation of China (Grant No. 62335006, 62022032, 62275065, and 61875047), Key Laboratory of Opto-Electronic Information Acquisition and Manipulation (Anhui University), Ministry of Education (Grant No. OEIAM202202), Fundamental Research Funds for the Central Universities (Grant No. HIT.OCEF.2023011).

References

[1] X.F. Wu, Y.M. Feng, G.D. Xu, Y.Q. Zhu, P.J. Ming, L.M. Dai, Numerical investigations on charge motion and combustion of natural gas-enhanced ammonia in marine pre-chamber lean-burn engine with dual-fuel combustion system, Int. J. Hydrog. Energy 48 (30) (2023) 11476–11492.
[2] F. Liu, D. Diercks, A.M. Hussain, N. Dale, Y. Furuya, Y. Miura, Y. Fukuyama, C. C. Duan, Nanocomposite catalyst for high-performance and durable intermediate-temperature methane-fueled metal-supported solid oxide fuel cells, ACS Appl. Mater. Interfaces 14 (48) (2022) 53840–53849.
[3] C. De Geyter, K. Van de Maele, B. Hauser, Y. Vandenplas, Hydrogen and methane breath test in the diagnosis of lactose intolerance, Nutrients 13 (9) (2021) 3261.
[4] D. Polag, F. Keppler, Effect of immune responses on breath methane dynamics, J. Breath. Res. 17 (4) (2023) 046005.
[5] J.C. Li, Y. Gao, L.G. Dou, C. Zhang, J. Du, T. Shao, Parametric investigations on plasma-activated conversion of CH_4–CH_3OH to C_2–C_4 alcohols by nanosecond pulsed discharge, Plasma Process. Polym. 20 (2) (2023) e2200162.
[6] T.W. Kim, H. Jeong, D. Kim, Y. Jo, H.J. Jung, J.H. Park, Y.W. Suh, Feasible coupling of CH_4/H_2 mixtures to H_2 storage in liquid organic hydrogen carrier systems, J. Power Sources 541 (2022) 231721.
[7] X.Y. Zhao, K. Chen, D.Y. Cui, M. Guo, C.X. Li, H.C. Qi, G.Y. Zhang, Z.F. Gong, Z. Zhou, W. Peng, Ultra-high sensitive photoacoustic gas detector based on differential multi-pass cell, Sens. Actuator B-Chem. 368 (2022) 132124.
[8] T.F. Stocker, D. Qin, G.K. Plattner, M. Tignor, S.K. Allen, J. Boschung, A. Nauels, Y. Xia, V. Bex and P.M. Midgley (eds.), IPCC, 2013: Climate Change 2013: The Physical Science Basis. Contribution of Working Group I to the Fifth Assessment Report of the Intergovernmental Panel on Climate Change, Cambridge University Press, Cambridge, United Kingdom and New York, NY, USA, (2014) 1535.
[9] X. Lan, K.W. Thoning, E.J. Dlugokencky, Trends in globally-averaged CH4, N2O, and SF6 determined from NOAA Global Monitoring Laboratory measurements, Version 2023–09, https://doi.org/10.15138/P8XG-AA10 2023.
[10] G. Etiope, R.W. Klusman, Geologic emissions of methane to the atmosphere, Chemosphere 49 (8) (2002) 777–789.
[11] Q.Q. Hao, Z.M. Luo, T. Wang, C. Xie, S.Q. Zhang, M.S. Bi, J. Deng, The flammability limits and explosion behaviours of hydrogen-enriched methane-air mixtures, Exp. Therm. Fluid Sci. 126 (2021) 110395.
[12] K. Hashimoto, T. Nakamura, T. Kageyama, V.R. Badarla, H. Shimada, R. Horisaki, T. Ideguchi, Upconversion time-stretch infrared spectroscopy, Light Sci. Appl. 12 (2023) 48.
[13] S.L. Jiang, F.F. Chen, Y. Zhao, S.F. Gao, Y.Y. Wang, H.L. Ho, W. Jin, Broadband all-fiber optical phase modulator based on photo-thermal effect in a gas-filled hollow-core fiber, Opto Electron. Adv. 6 (5) (2023) 220085.
[14] T. Wang, J.F. Jiang, K. Liu, S. Wang, P.P. Niu, Y.Z. Liu, T.G. Liu, Flexible minimally invasive coherent anti-Stokes Raman spectroscopy (CARS) measurement method with tapered optical fiber probe for single-cell application, PhotoniX 3 (1) (2022) 11.
[15] Z.D. Zhang, T. Peng, X.Y. Nie, G.S. Agarwal, M.O. Scully, Entangled photons enabled time-frequency-resolved coherent Raman spectroscopy and applications to electronic coherences at femtosecond scale, Light Sci. Appl. 11 (2022) 274.
[16] J.H. van Helden, N. Lang, U. Macherius, H. Zimmermann, J. Ropcke, Sensitive trace gas detection with cavity enhanced absorption spectroscopy using a continuous wave external-cavity quantum cascade laser, Appl. Phys. Lett. 103 (13) (2013) 131114.
[17] B.X. Xu, X.Y. Fan, S. Wang, Z.Y. He, Sub-femtometer-resolution absolute spectroscopy with sweeping electro-optic combs, Opto Electron. Adv. 5 (12) (2022) 210023.
[18] W. Yang, F. Knorr, I. Latka, M. Vogt, G.O. Hofmann, J. Popp, I.W. Schie, Real-time molecular imaging of near-surface tissue using Raman spectroscopy, Light Sci. Appl. 11 (1) (2022) 90.
[19] J.X. Yi, H. Zhang, Z.B. Zhang, D.D. Chen, Hierarchical porous hollow SnO_2 nanofiber sensing electrode for high performance potentiometric H_2 sensor, Sens. Actuator B-Chem. 268 (2018) 456–464.
[20] Y.F. Qi, Y.H. Liu, J.B. Luo, Recent application of Raman spectroscopy in tumor diagnosis: from conventional methods to artificial intelligence fusion, PhotoniX 4 (1) (2023) 22.
[21] M. Vlk, A. Datta, S. Alberti, H.D. Yallew, V. Mittal, G.S. Murugan, J. Jagerska, Extraordinary evanescent field confinement waveguide sensor for mid-infrared trace gas spectroscopy, Light Sci. Appl. 10 (2021) 26.
[22] A. Leal-Junior, L. Avellar, V. Biazi, M.S. Soares, A. Frizera, C. Marques, Multifunctional flexible optical waveguide sensor: on the bioinspiration for ultrasensitive sensors development, Opto Electron. Adv. 5 (10) (2022) 210098.
[23] J.M. Le, Y.D. Su, C.S. Tian, A.H. Kung, Y.R. Shen, A novel scheme for ultrashort terahertz pulse generation over a gapless wide spectral range: Raman-resonance-enhanced four-wave mixing, Light Sci. Appl. 12 (1) (2023) 34.
[24] Y.H. Liu, Y.F. Ma, Advances in multipass cell for absorption spectroscopy-based trace gas sensing technology, Chin. Opt. Lett. 21 (3) (2023) 033001.
[25] Z.G. Chen, M. Segev, Highlighting photonics: looking into the next decade, eLight 1 (1) (2021) 2.
[26] Y. He, Y.F. Ma, Y. Tong, X. Yu, F.K. Tittel, Ultra-high sensitive light-induced thermoelastic spectroscopy sensor with a high Q-factor quartz tuning fork and a multipass cell, Opt. Lett. 44 (8) (2019) 1904–1907.
[27] C. Zhang, S.D. Qiao, Y. He, S. Zhou, L. Qi, Y.F. Ma, Differential quartz-enhanced photoacoustic spectroscopy, Appl. Phys. Lett. 122 (24) (2023) 241103.
[28] L.Y. Yang, Y.P. Li, F. Fang, L.Y. Li, Z.J. Yan, L. Zhang, Q.Z. Sun, Highly sensitive and miniature microfiber-based ultrasound sensor for photoacoustic tomography, Opto Electron. Adv. 5 (6) (2022) 200076.
[29] X.Y. Zhao, C.X. Li, H.C. Qi, J.Y. Huang, Y.F. Xu, Z.Z. Wang, X. Han, M. Guo, K. Chen, Integrated near-infrared fiber-optic photoacoustic sensing demodulator for ultra-high sensitivity gas detection, Photoacoustics 33 (2022) 100560.
[30] W.P. Chen, S.D. Qiao, Z.X. Zhao, S.F. Gao, Y.Y. Wang, Y.F. Ma, Sensitive carbon monoxide detection based on laser absorption spectroscopy with hollow-core antiresonant fiber, Microw. Opt. Technol. Lett. 66 (1) (2024) e33780.
[31] Y.Q. Wang, J.H. Zhang, Y.C. Zheng, Y.R. Xu, J.Q. Xu, J. Jiao, Y. Su, H.F. Lv, K. Liang, Brillouin scattering spectrum for liquid detection and applications in oceanography, Opto Electron. Adv. 6 (1) (2023) 220016.
[32] A. Li, C. Wang, F.X. Bao, W.J. Fang, Y.X. Liang, R. Cheng, S.L. Pan, An integrated single-shot spectrometer with large bandwidth-resolution ratio and wide operation temperature range, PhotoniX 4 (1) (2023) 29.
[33] A.A. Kosterev, Y.A. Bakhirkin, R.F. Curl, F.K. Tittel, Quartz-enhanced photoacoustic spectroscopy, Opt. Lett. 27 (21) (2002) 1902–1904.
[34] S.S. Sunandana, Physical applications of photoacoustic-spectroscopy, Phys. Status Solidi A-Appl. Mat. 105 (1) (1988) 11–43.
[35] Y. Cao, R.F. Wang, J. Peng, K. Liu, W.D. Chen, G.S. Wang, X.M. Gao, Humidity enhanced N_2O photoacoustic sensor with a 4.53 μm quantum cascade laser and Kalman filter, Photoacoustics 24 (2021) 100303.
[36] Y.F. Ma, R. Lewicki, M. Razeghi, F.K. Tittel, QEPAS based ppb-level detection of CO and N_2O using a high power CW DFB-QCL, Opt. Express 21 (1) (2013) 1008–1019.
[37] X.N. Liu, S.D. Qiao, G.W. Han, J.X. Liang, Y.F. Ma, Highly sensitive HF detection based on absorption enhanced light-induced thermoelastic spectroscopy with a

quartz tuning fork of receive and shallow neural network fitting, Photoacoustics 28 (2022) 100422.
[38] S.D. Qiao, P.Z. Ma, V. Tsepelin, G.W. Han, J.X. Liang, W. Ren, H.D. Zheng, Y.F. Ma, Super tiny quartz-tuning-fork-based light-induced thermoelastic spectroscopy sensing, Opt. Lett. 48 (2) (2023) 419–422.
[39] Y.F. Ma, Y.Q. Hu, S.D. Qiao, Z.T. Lang, X.N. Liu, Y. He, V. Spagnolo, Quartz tuning forks resonance frequency matching for laser spectroscopy sensing, Photoacoustics 25 (2022) 100329.
[40] C. Zhang, Y. He, S.D. Qiao, Y.F. Ma, Differential integrating sphere based photoacoustic spectroscopy gas sensing, Opt. Lett. 48 (19) (2023) 5089–5092.
[41] H.J. Luo, Z.F. Yang, R.B. Zhuang, H.H. Lv, C.L. Wang, H.Y. Lin, D. Zhang, W. G. Zhu, Y.C. Zhong, Y. Cao, K. Liu, R.F. Kan, Y.W. Pan, J.H. Yu, H.D. Zheng, Ppbv-level mid-infrared photoacoustic sensor for mouth alcohol test after consuming lychee fruits, Photoacoustics 33 (2023) 100559.
[42] X.Y. Zhao, M. Guo, D.Y. Cui, C.X. Li, H.C. Qi, K. Chen, F.X. Ma, J.Y. Huang, G. Y. Zhang, J.K. Zhao, Multi-pass differential photoacoustic sensor for real-time measurement of SF_6 decomposition component H_2S at the ppb level, Anal. Chem. 95 (21) (2023) 8214–8222.
[43] C. Zhang, S.D. Qiao, Y.F. Ma, Highly sensitive photoacoustic acetylene detection based on differential photoacoustic cell with retro-reflection-cavity, Photoacoustics 30 (2023) 100467.
[44] X.N. Liu, Y.F. Ma, Sensitive carbon monoxide detection based on light-induced thermoelastic spectroscopy with a fiber-coupled multipass cell, Chin. Opt. Lett. 20 (3) (2022) 031201.
[45] X.N. Liu, Y.F. Ma, New temperature measurement method based on light-induced thermoelastic spectroscopy, Opt. Lett. 48 (21) (2023) 5687–5690.
[46] Y.X. Zhang, Y.Z. Li, Z.H. Song, R. Lin, Y.F. Chen, J.Q. Qian, A high-Q AFM sensor using a balanced trolling quartz tuning fork in the liquid, Sensors 18 (5) (2018) 1628.
[47] C. Fang, T.T. Liang, S.D. Qiao, Y. He, Z.C. Shen, Y.F. Ma, Quartz-enhanced photoacoustic spectroscopy sensing based on novel quartz tuning forks, Opt. Lett. (2024), https://doi.org/10.1364/OL.513628.
[48] Y.F. Ma, Y. He, Y. Tong, X. Yu, F.K. Tittel, Quartz-tuning-fork enhanced photothermal spectroscopy for ultra-high sensitive trace gas detection, Opt. Express 26 (24) (2018) 32103–32110.
[49] H.P. Wu, L. Dong, H.D. Zheng, Y.J. Yu, W.G. Ma, L. Zhang, W.B. Yin, L.T. Xiao, S. T. Jia, F.K. Tittel, Beat frequency quartz-enhanced photoacoustic spectroscopy for fast and calibration-free continuous trace-gas monitoring, Nat. Commun. 8 (2017) 15331.
[50] A. Zifarelli, R. De Palo, P. Patimisco, M. Giglio, A. Sampaolo, S. Blaser, J. Butet, O. Landry, A. Müller, V. Spagnolo, Multi-gas quartz-enhanced photoacoustic sensor for environmental monitoring exploiting a Vernier effect-based quantum cascade laser, Photoacoustics 28 (2022) 100401.
[51] Z.T. Lang, S.D. Qiao, T.T. Liang, Y. He, L. Qi, Y.F. Ma, Dual-frequency modulated heterodyne quartz-enhanced photoacoustic spectroscopy, Opt. Express 32 (1) (2024) 379–386.
[52] Z.T. Lang, S.D. Qiao, Y.F. Ma, Fabry–Perot-based phase demodulation of heterodyne light-induced thermoelastic spectroscopy, Light Adv. Manuf 4 (2023) 23.
[53] Y.F. Ma, T.T. Liang, S.D. Qiao, X.N. Liu, Z.T. Lang, Highly sensitive and fast hydrogen detection based on light-induced thermoelastic spectroscopy, Ultrafast Sci. 3 (2023) 0024.
[54] D. Lu, Q.L. Yang, H. Wang, Y.M. He, H.F. Qi, H. Wang, L.J. Zhao, W. Wang, Review of semiconductor distributed feedback lasers in the optical communication band, Chin. J. Lasers 47 (7) (2020) 0701001.
[55] Y.J. Chen, T.T. Liang, S.D. Qiao, Y.F. Ma, A miniaturized 3D-printed quartz-enhanced photoacoustic spectroscopy sensor for methane detection with a high-power diode laser, Sensors 23 (8) (2023) 4034.
[56] K. Chan, H. Ito, H. Inaba, All-optical-fiber-based remote-sensing system for near-infrared absorption of low-level CH_4, Gas., J. Light. Technol. 5 (12) (1987) 1706–1711.
[57] I.E. Gordon, L.S. Rothman, R.J. Hargreaves, R. Hashemi, E.V. Karlovets, F. M. Skinner, E.K. Conway, C. Hill, R.V. Kochanov, Y. Tan, et al., The HITRAN2020 molecular spectroscopic database, J. Quant. Spectrosc. Radiat. Transf. 277 (2022) 107949.
[58] W.P. Chen, S.D. Qiao, Z.T. Lang, J.C. Jiang, Y. He, Y.W. Shi, Y.F. Ma, Hollow-waveguide-based light-induced thermoelastic spectroscopy sensing, Opt. Lett. 48 (15) (2023) 3989–3992.
[59] Y.F. Ma, Y. He, X. Yu, J.B. Zhang, R. Sun, F.K. Tittel, Compact all-fiber quartz-enhanced photoacoustic spectroscopy sensor with a 30.72 kHz quartz tuning fork and spatially resolved trace gas detection, Appl. Phys. Lett. 108 (2016) 091115.
[60] K. Liu, X.Y. Guo, H.M. Yi, W.D. Chen, W.J. Zhang, X.M. Gao, Off-beam quartz-enhanced photoacoustic spectroscopy, Opt. Lett. 34 (10) (2009) 1594–1596.
[61] L. Dong, A.A. Kosterev, D. Thomazy, F.K. Tittel, QEPAS spectrophones: design, optimization, and performance, Appl. Phys. B-Lasers Opt. 100 (3) (2010) 627–635.
[62] Y.F. Ma, Y.H. Hong, S.D. Qiao, Z.T. Lang, X.N. Liu, H-shaped acoustic micro-resonator-based quartz-enhanced photoacoustic spectroscopy, Opt. Lett. 47 (3) (2022) 601–604.
[63] J.C. Sun, J. Chang, F.P. Wang, Q.D. Zhang, Z.L. Wang, Y.L. Xie, Z.W. Zhang, Y. W. Feng, Tuning efficiency of distributed feedback laser diode for wavelength modulation spectroscopy, IEEE Sens. J. 19 (21) (2019) 9722–9727.
[64] H.M. Yi, K. Liu, S.W. Sun, W.J. Zhang, X.M. Gao, Theoretical analysis of off beam quartz-enhanced photoacoustic spectroscopy sensor, Opt. Commun. 285 (24) (2012) 5306–5312.
[65] D.V. Land, A.P. Levick, J.W. Hand, The use of the Allan deviation for the measurement of the noise and drift performance of microwave radiometers, Meas. Sci. Technol. 18 (7) (2007) 1917–1928.
[66] L. Dong, J. Wright, B. Peters, B.A. Ferguson, F.K. Tittel, S. McWhorter, Compact QEPAS sensor for trace methane and ammonia detection in impure hydrogen, Appl. Phys. B-Lasers Opt. 107 (2) (2012) 459–467.
[67] Y. Li, R.Z. Wang, F.K. Tittel, Y.F. Ma, Sensitive methane detection based on quartz-enhanced photoacoustic spectroscopy with a high-power diode laser and wavelet filtering, 132 (2020) 106155.
[68] C. Lin, X.Y. Yan, Y.C. Huang, An all-optical off-beam quartz-enhanced photoacoustic spectroscopy employing double-pass acoustic microresonators, Opt. Commun. 503 (2022) 127447.
[69] G. Menduni, A. Zifarelli, E. Kniazeva, S. Dello Russo, A.C. Ranieri, E. Ranieri, P. Patimisco, A. Sampaolo, M. Giglio, F. Manassero, et al., Measurement of methane, nitrous oxide and ammonia in atmosphere with a compact quartz-enhanced photoacoustic sensor, Sens. Actuator B-Chem. 375 (2023) 132953.
[70] A. Zifarelli, G. Menduni, M. Giglio, A. Elefante, A. Sukhinets, A. Sampaolo, P. Patimisco, F.Y. Sun, C.W. Wang, J.W. Qi, V. Spagnolo, Compact and versatile QEPAS-based sensor box for simultaneous detection of methane and infrared absorber gas molecules in ambient air, Front. Environ. Chem. 3 (2022) 926233.
[71] A. Sampaolo, G. Menduni, P. Patimisco, M. Giglio, V.M.N. Passaro, L. Dong, H. P. Wu, F.K. Tittel, V. Spagnolo, Quartz-enhanced photoacoustic spectroscopy for hydrocarbon trace gas detection and petroleum exploration, Fuel 277 (2020) 118118.
[72] H.P. Wu, L. Dong, X.K. Yin, A. Sampaolo, P. Patimisco, W.G. Ma, L. Zhang, W. B. Yin, L.T. Xiao, V. Spagnolo, et al., Atmospheric CH_4 measurement near a landfill using an ICL-based QEPAS sensor with V-T relaxation self-calibration, Sens. Actuator B-Chem. 297 (2019) 126753.
[73] M. Jahjah, W. Ren, P. Stefański, R. Lewicki, J.W. Zhang, W.Z. Jiang, J. Tarka, F. K. Tittel, A compact QCL based methane and nitrous oxide sensor for environmental and medical applications, Analyst 139 (9) (2014) 2065–2069.
[74] W.L. Ye, W.H. Liu, W.X. Luo, J.S. Xiao, L.F. He, Y.F. Huang, D.Y. Zhu, Calibration-free near-infrared methane sensor system based on BF-QEPAS, Infrared Phys. Technol. 133 (2023) 104784.

Tiantian Liang received his B.S. degree in optoelectronic information science and engineering from Yanshan University, China, in 2021. Then, he received his M.S. degree in physical electronics from Harbin Institute of Technology in 2023. He is now pursuing a PhD degree in physical electronics from Harbin Institute of Technology. His research interest is focused on photoacoustic spectroscopy and the design of quartz tuning fork.

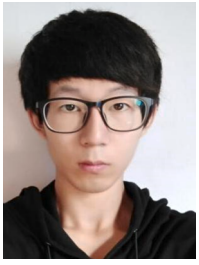

Shunda Qiao received his B.S. degree in electronic science and technology from Yanshan University, China, in 2018. In 2020, he received his M.S. degree and began to pursue a PhD degree of physical electronics from Harbin Institute of Technology. His research interests include photoacoustic spectroscopy and its applications.

Yanjun Chen received his bachelor's degree in electronic science and technology from Harbin Institute of Technology in 2023. In the same year he pursued a master's degree in physical electronics from Harbin Institute of Technology. His main research area is quartz-enhanced photoacoustic spectroscopy

Ying He obtained his master's and doctorate degrees in physical electronics from Harbin Institute of Technology in 2017 and 2022, respectively. Currently, he is an associate professor at the Harbin Institute of Technology, China. His research interests including trace gas sensing based on QEPAS, LITES and other laser spectroscopy.

Yufei Ma received his PhD degree in physical electronics from Harbin Institute of Technology, China, in 2013. From September 2010 to September 2011, he spent as a visiting scholar at Rice University, USA. Currently, he is a professor at Harbin Institute of Technology, China. He is the winner of National Outstanding Youth Science Fund. His research interests include optical sensors, trace gas detection, laser spectroscopy, solid-state laser and optoelectronics. He has published more than 100 publications and given more than 20 invited presentations at international conferences. He serves as associate editor for Optica *Optics Express*, SPIE *Optical Engineering*, Wiley *Microwave and Optical Technology Letters* and *Frontiers in Physics*. He also serves as topical editor for CLP *Chinese Optics Letters* and editorial board member for Elsevier *Photoacoustics* MDPI *Sensors* and *Applied Sciences*.